Atmospheric Environment 254 (2021) 118373

Contents lists available at ScienceDirect

Atmospheric Environment

journal homepage: http://www.elsevier.com/locate/atmosenv

Valine involved sulfuric acid-dimethylamine ternary homogeneous nucleation and its atmospheric implications

Ying Liu [a], Yi-Rong Liu [a,**], Ya-Juan Feng [a], Teng Huang [b], Shuai Jiang [a], Zi-Hang Wang [a], Hui Cao [a], Wei Huang [a,b,c,*]

[a] School of Information Science and Technology, University of Science and Technology of China, Hefei, Anhui, 230026, China
[b] Laboratory of Atmospheric Physico-Chemistry, Anhui Institute of Optics & Fine Mechanics, Chinese Academy of Sciences, Hefei, Anhui, 230031, China
[c] Center for Excellent in Urban Atmospheric Environment, Institute of Urban Environment, Chinese Academy of Sciences, Xiamen, Fujian, 361021, China

HIGHLIGHTS

- The possibility of Valine participating in the formation of new particles in the urban-suburban environment.
- A new formation routes mode has been generated with the existence of VAL compared with pure SA-DMA.
- Valine may play a more important role in the growth stage than the initial nucleation stage.
- Lower temperature could promote the formation of clusters.

ARTICLE INFO

Keywords:
Nucleation mechanism
Amino acid
Topological analysis
Evaporation rate
Atmospheric relevance

ABSTRACT

New Particle Formation (NPF) is considered as the dominant source of aerosol particles, influencing the environment and human health tightly. In recent years, valine (VAL) has been identified in field detection in urban areas, which reveals that VAL may play an important role in participating in atmospheric nucleation. However, there have been no categorical reports explaining how VAL participates in the multi-component nucleation with precursor Sulfuric Acid (SA) and the atmospheric organic amine Dimethylamine (DMA) so far. In this paper, quantum chemical calculation and cluster kinetic simulation have been studied to research the nucleation mechanism of $(SA)_x(DMA)_y(VAL)_z$ ($0 \leq x, y, z \leq 3$) system. Structural and thermodynamic analysis at ωB97XD/6-31++G(d, p) theory level and basis set shows that VAL could form various stable structures through hydrogen bonds with SA and DMA, and proton transfer in ternary structure enhances the stability of system. However, in the clusters of SA-DMA-VAL system with large numbers of molecules, there has been steric hindrance between molecules of cluster due to the high proportion of inactive groups in VAL, which insulates the further formation of hydrogen bonds. With regard to the distribution of Gibbs free energy on VAL-DMA grid, the energy decreases rapidly along the diagonal with VAL and DMA in different numbers of SA molecules, predicting possible nucleation path along the diagonal. Besides, there is a synergistic effect of VAL in system SA-DMA-VAL, and VAL tends to replace the role of DMA in the ternary system. Evaporation rate analysis indicates that the ternary system containing SA is more stable. The simulating formation rate of SA-DMA-VAL system compared with the CLOUD experiment at CERN shows that the nucleation potential of SA-DMA-VAL is superior to that of SA-NH_3-H_2O, but inferior to that of SA-DMA-H_2O, inferring that VAL may show more potential in growth processes than the initial nucleation processes in the light of the specific value of formation rate.

1. Introduction

Atmospheric aerosols have brought a wide and profound impact on the global climate balance through direct climate forcing or indirect climate forcing (Charlson et al., 1992a, 1992b; Haywood and Ramaswamy, 1998; Raes et al., 2000; Satheesh and Krishna Moorthy, 2005),

* Corresponding author. School of Information Science and Technology, University of Science and Technology of China, Hefei, Anhui, 230026, China.
** Corresponding author.
E-mail addresses: yrliu@ustc.edu.cn (Y.-R. Liu), huangwei6@ustc.edu.cn (W. Huang).

https://doi.org/10.1016/j.atmosenv.2021.118373
Received 24 November 2020; Received in revised form 21 March 2021; Accepted 24 March 2021
Available online 31 March 2021

influencing the weather, visibility, air quality, and public health (Meehl, 1996; Rosser et al., 2020; Saxon and Diaz-Sanchez, 2005; Smith et al., 2017). It is reported that the transmission of global coronavirus disease 2019(COVID-19) via aerosols can spread a more extended distance and time than contact spread (Zhang et al., 2020). Generally, new particle formation (NPF) is considered as a dominant source of atmospheric aerosol particles in terms of the number concentration at the global scale (Kecorius et al., 2019; Wendisch et al., 2019; Zhang et al., 2012).

There have been great quantities of field measurement and laboratory simulations reported on NPF currently (Kerminen et al., 2018; Kulmala et al., 2004; Lee et al., 2019; Wu et al., 2007). Various nucleation mechanisms have been proposed, such as binary nucleation, ternary nucleation, ion-induced nucleation, and iodine oxide nucleation, etc. (Kulmala et al., 2000; Kürten et al., 2015; O'Dowd et al., 2002b; Yu and Turco, 2000) However, sulfuric acid (SA) is generally considered as the key species in NPF (Boy et al., 2005). Experimental data confirmed that the NPF event is related to the concentration of SA vapor (Sipilä et al., 2010). However, SA concentration is not enough to explain the NPF observed in the field measurement (Berndt et al., 2005; Kerminen et al., 2010; Kuang et al., 2008). Zhang et al. have pointed out that there are two processes in the occurrence of nucleation events (Kulmala, 2003), the initial small cluster grows very slowly until a critical size cluster is formed, then the cluster grows in size by SA condensation and is simultaneously stabilized by amines, ammonia, or organic vapors, at last, the cluster could grow rapidly to a detected size (Almeida et al., 2013; Kirkby et al., 2011). It has been verified that amines can enhance nucleation, stabilize clusters and reduce evaporation, which could be explained by a base-stabilization mechanism involving acid-amine pairs (Almeida et al., 2013; Kulmala et al., 2013; Kürten et al., 2014). Dimethylamine (DMA) is one of the most abundant aliphatic amines in ambient particles (Kuwata et al., 1983). DMA has lower volatility compared with NH_3, and has a stronger enhancement effect in the nucleation of sulfuric acid in the presence of water (W) (Ge et al., 2011; Loukonen et al., 2010; Youn et al., 2015). Almeida et al. indicated that particle formation rates could increase by up to 1,000-fold when the concentration of DMA above three parts per trillion by volume compared with ammonia using the CLOUD chamber at CERN, partially explaining the fast particle formation rate observed in the atmosphere (Almeida et al., 2013). A recent measurement result by Jasper et al. revealed that the concentration level of DMA in the environment was of considerable variability (Almeida et al., 2013; Kirkby et al., 2011). In such cases, the binary isotropic nucleation of DMA and SA in the presence of W was still insufficient to explain the reported nucleation rate in the low DMA concentration region, which indicated that there were other atmospheric vapors involved in nucleation (Zhang et al., 2004). Numerous reports indicated that low volatile highly oxidized organic molecules (HOM), organic acids, and nitrogen-containing organic compounds were involved in nucleation (Ehn et al., 2014; O'Dowd et al., 2002a; Zhang et al., 2004).

Nitrogen-containing compounds account for a large proportion of amines (Cornell, 2011). In addition, amino acids are also important components of nitrogen-containing compounds (Cornell et al., 2003). Abundant amino acids were found in the atmosphere of the Antarctic Arctic, cities, plains, rural areas, and oceans (Barbaro et al., 2011; Feltracco et al., 2019; McGregor and Anastasio, 2001). More than 30 amino acids were detected in rainwater and atmospheric particles, and these amino acids are usually in the form of free amino acids or combined amino acids (Ge et al., 2011). Martin reported that combined amino acids (CAA) and free amino acids (FAA) are enriched up to 50 types in marine surface water (Wedyan and Preston, 2008). Free and combined amino acids are important components of water-soluble organic nitrogen (DON) in rainwater and aerosols, occupying 20-50% of the total content (Cornell, 2011; Zhang and Anastasio, 2003). Amino acids derived from human activities were thought to derive from biological proteins and biomass burning, promoting the formation of secondary aerosols (De Haan et al., 2009). Considering their atmospheric abundance, amino acids are speculated to participate in the formation of new particles serving as potential nucleation stabilizers (Wedyan and Preston, 2008). In addition, field investigations proved that the free amino acids in the aerosol showed an obvious seasonal correlation (Ren et al., 2018; Xu et al., 2019), which is consistent with the seasonality of the aerosol CCN (Asmi et al., 2016; Charlson et al., 2001; Merikanto et al., 2009). Amino acids can change the order and aggregation of water molecules through their hydrophilic groups, amino groups, carboxyl groups, and side chains, promoting the growth of hydrates. Free amino acids can preserve water even at low Relative Humidity (RH) for its hygroscopicity and could be involved in efficient cloud condensation nuclei formation (Chan et al., 2005; Di Filippo et al., 2014). At the same time, there are both carboxyl groups and amino groups in the molecules of amino acids, similar to the reports of enhanced nucleation in the two acid directions of dicarboxylic acids, this property makes the amino acids involved in nucleation could also combine other molecules from two directions (Arquero et al., 2017; Xu and Zhang, 2012). Therefore, it is meaningful to study the involvement of amino acids in nucleation for further understanding of atmospheric nucleation. So far, there have been some theoretical nucleation calculations about common amino acids. The interaction of serine and threonine with SA and W has been studied by Pu Ge (Ge et al., 2018). Threonine can interact with SA and W in three directions, and Threonine plays an important role in stabilizing sulfuric acid. Glycine has been shown to enhance its interaction with aerosol precursors through its inherent amphoteric nature to form a protonated state when interacting with atmospheric nucleation precursors W, NH3, SA (Elm et al., 2013b).

In the aerosol collected in Beijing from 2012 to 2013, VAL was detected to be one of the three most abundant amino acids, and these three amino acids accounted for 46% of the total amino acids (Ren et al., 2018). Four PM2.5 samples collected in Nanjing in February 2001 came to the same conclusion, the concentration of VAL is among the top 3 (Yang et al., 2005). Rich protein and FAA were detected in fine particulate matter samples in rural areas of Guangzhou. Among FAA, VAL accounted for 18.5%, slightly lower than glycine(Song et al., 2017) (19.9%). However, the concentration of VAL in amino acid samples collected in the Arctic and marine regions was not as rich as that detected in cities and suburbs (Feltracco et al., 2019). This indicates that studying the nucleation of VAL is of great significance to reveal the nucleation process of aerosols in cities and rural areas away from the ocean and Polar region (Matsumoto and Uematsu, 2005).

Research on atmosphere amino acids involved with atmospheric nucleation precursors is numerous (Barbaro et al., 2011; Kristensson et al., 2010; Milne and Zika, 1993; Sun et al., 2013), however, the study of VAL with the participation of acids and bases at the molecular level is rare. In this paper, the ternary nucleation of VAL and sulfate-amine systems was studied by molecular dynamics simulation on the basis of the ωB97XD/6-31++G (d, p) method using the density functional (DFT) method. The lowest energy structures of these different clusters were calculated, and the thermodynamic properties and temperature dependence, and concentration dependence of these clusters were analyzed in this work.

2. Method

2.1. Thermodynamics calculations

Basin-Hopping (BH) algorithm coupled with semi-empirical PM7 implemented in MOPAC 2016 were used to search all the low energy geometries of clusters $(SA)_x(DMA)_y(VAL)_z$ ($0 \leq x, y, z \leq 3$) (Hostaš et al., 2013; Huang et al., 2010), our previous calculation has proven that this method is effective in predicting equilibrium structures, thermodynamics, and properties of molecular and atomic systems (Hou et al., 2016; Jiang et al., 2014; Liu et al., 2014; Wales and Doye, 1997). The following two steps were executed to obtain the minimum energy configuration of each size cluster: Firstly, displace single molecular

randomly to generate configurations in the cluster, and the semi-empirical PM7 method was then used to optimize the structures to a local minimum (Hostaš et al., 2013). The local minimum was considered to be characterized when the final search result shows the same value three times (Xu et al., 2020). Secondly, the optimized local energy minimum was used as a criterion, if the energy of current newly generated structure was lower than it, the local energy minimum would be replaced with the current energy, otherwise, accept initial generated structure spaces with Boltzmann weight at a finite temperature (Liu et al., 2014).

The isomers obtained by the BH method were then sorted according to relative energy. The top 30 isomers with the low energy were selected for each cluster, and then, these structures were further optimized at the theory level of ωB97XD function and 6-31++G (d, p) basis set. Harmonic vibrational frequency calculations were operated for each stationary low-lying structure to guarantee no imaginary frequencies. Geometry optimization and frequency calculation are all carried out on the Gaussian 09 program package (Frisch et al., 2013). Single point energy was calculated at DLPNO-CCSD(T)/aug-cc-pVTZ theory level and basis set used the ORCA 4.0 suite of programs (Neese, 2018; Riplinger and Neese, 2013).

The ωB97XD functional was frequently chosen in calculating the binding energy of atmospheric clusters for its good performance (Elm et al., 2013a; Xie et al., 2017). Theoretical results and the experimental data has verified that ωB97XD yielded the lowest mean absolute error and maximum errors below 1 kcal mol^{-1} with a test set of atmospherically relevant clusters compared to DF-LCCSD(T)-F12a/VDZ-F12 and CCSD. To prove the correctness of choosing ωB97XD functional, some more accurate density functional (M06-2X, PW91PW91, ωB97XD, B3LYP) were compared with high-precision density functional of MP2 in Gibbs free energy change, the benchmark result (Table S1) demonstrated that ωB97XD functional shows very good accuracy and consistency with MP2 functional. Meanwhile, the 6-31++G(d, p) basis set is a compromise between efficiency and accuracy, which represents a cost-effective methodology, thus it was utilized in this study (Xie et al., 2017).

2.2. Kinetic calculations

Here, we used the birth-death equations (BDE) proposed by McGrath (McGrath et al., 2012; Ortega et al., 2012) to describe the growth process of the clusters, which described the collision coefficient of molecular clusters, and the formation free energies of SA-DMA-VAL clusters calculated by quantum chemical methods were used to obtain the clusters evaporation rate coefficient. Finally, the condensation and evaporation of molecular clusters were comprehensively considered to obtain the formation rate of clusters.

Friedlander et al. have given the collision rate $\beta_{i,j}$ by kinetic gas theory as(Licht and Friedlander, 1977):

$$\beta_{i,j} = \left(\frac{3}{4\pi}\right)^{1/6} \left(\frac{6k_bT}{m_i} + \frac{6k_bT}{m_j}\right)^{1/2} \left(V_i^{1/3} + V_j^{1/3}\right)^2 \quad (1)$$

$\beta_{i,j}$ represents the collision rate of two clusters i and j, where m_i and m_j are the masses of cluster i and cluster j, V_i and V_j are their respective volumes, k_b is the Boltzmann constant, and T refers to the temperature. The evaporation rate can be calculated from the above collision coefficient and thermodynamic parameter as follows (Ortega et al., 2011):

$$\gamma_{(i+j)\rightarrow i,j} = \beta_{i,j} c_{ref} \exp\left(\frac{\Delta G_{i+j} - \Delta G_i - \Delta G_j}{k_bT}\right) \quad (2)$$

$\gamma_{(i+j)\rightarrow i,j}$ represents the evaporation rate of cluster i and j from the cluster evaporation of i+j, where ΔG_{i+j}, ΔG_i, ΔG_j are the Gibbs free energies of formation of clusters i + j, i and j from monomers at reference pressure c_{ref} The corresponding Gibbs free energy is zero if the cluster is a monomer. c_{ref} is a temperature-dependent parameter, resulting in the evaporation rate a temperature-dependent value as well. Studies has shown that temperature change has a significant effect on the steady-state concentration of all clusters.

From the collision coefficient and evaporation rate of the cluster, the time development of molecular cluster distributions at different concentrations c_i can be further described by the analysis of the dynamic code of the atmospheric cluster (ACDC), which can be explicitly solved by the birth-death equations as follows[72]:

$$\frac{d_{c_i}}{dt} = \frac{1}{2}\sum_{j<i} \boldsymbol{\beta}_{j,(i-j)} \boldsymbol{c}_j \boldsymbol{c}_{i-j} + \sum_j \boldsymbol{\gamma}_{(i+j)\rightarrow i} \boldsymbol{c}_{(i+j)} - \sum_j \boldsymbol{\beta}_{i,j} \boldsymbol{c}_i \boldsymbol{c}_j - \frac{1}{2}\sum_{j<i} \boldsymbol{\gamma}_{i\rightarrow j} \boldsymbol{c}_i + \boldsymbol{Q}_i - \boldsymbol{S}_i \quad (3)$$

3. Results and discussion

3.1. Structure analysis

Previous studies have shown that the stability of a cluster can be greatly affected by the strength of the molecular hydrogen bond and proton transfer, it seems that shorter hydrogen bonds and proton transfer could enhance cluster stability summarized from previous studies (Elm et al., 2016; Kollman and Allen, 1972). Here, the global minimum energy structures of clusters from $(SA)_x(DMA)_y(VAL)_z$ ($0 \leq x, y, z \leq 3$) were calculated and optimized at ωB97XD/6-31++G(d, p) level of theory and basis set in this study. Fig. 1 shows the most stable configurations of SA involved dimers and some key trimers. The structural information of other clusters is listed in Fig. S1.

As presented in Fig. 1, for binary clusters, it is obvious that SA and DMA are combined with two hydrogen bond and proton transfer occurs in $(SA)_1\cdot(DMA)_1$. A ring structure is formed in $(SA)_1\cdot(VAL)_1$ where VAL combines SA through two hydrogen bonds with the length of 1.737 Å and 1.544 Å, which is shorter than that of $(SA)_1\cdot(DMA)_1$ (1.680 Å and 1.738 Å), but no proton transfer occurs in the $(SA)_1\cdot(VAL)_1$ cluster. For the cluster of $(SA)_1\cdot(NH_3)_1$, there is only one hydrogen bond compared with the dimer of $(SA)_1\cdot(VAL)_1$. It is worth noting that the carboxyl group (-COOH) instead of the amino group ($-NN_2$) of VAL molecule combines with SA molecule in $(SA)_1\cdot(VAL)_1$, which differs from the structures of $(Ser)_1\cdot(SA)_1$, $(Thr)_1\cdot(SA)_1$ studied by Pu Ge(Ge et al., 2018), in which structures, hydroxyl group instead of the –COOH combines with the SA. These results indicate that amino acids molecules with different methyl groups would have different interaction patterns even though they have both amino and carboxyl functional groups.

When a VAL monomer is added to the cluster $(SA)_1\cdot(DMA)_1$, the initial ring structure of $(SA)_1\cdot(DMA)_1$ molecule is broken, then $(VAL)_1\cdot(SA)_1\cdot(DMA)_1$ cluster exhibits a three-membered ring with three hydrogen bonds of length 1.711 Å, 1.659 Å and 1.618 Å respectively, and proton transfer occurs between SA and DMA molecules. For the cluster of $(VAL)_2\cdot(SA)_1\cdot(DMA)_1$, the two VAL molecules are connected to SA and DMA through carboxyl and amino groups, respectively. Meanwhile, one hydrogen of SA in this cluster is transferred to DMA through proton transfer. The result verifies the previous conjecture that amino acids can combine with other molecule from both amino and carboxyl directions. When the number of VAL molecules increases to three, a more complex three-ring structure $(VAL)_3\cdot(SA)_1\cdot(DMA)_1$ is formed. In this system, proton transfer occurs among DMA, VAL, and SA molecules, and the VAL molecule acts as both hydrogen-bond acceptor and donor for proton transfer. In the other clusters listed in Fig. 1, either amino group or carboxyl group of VAL participates in the combination when the number of molecules involved in clusters is small, which may be related to space steric hindrance effect. The clusters centered on VAL occupies a larger space position due to the non-bonding group of VAL, which prevents the bonding group of SA and DMA from attacking the amino and carboxyl groups of VAL.

However, as the number of molecules increasing, both the two functional groups form hydrogen bonds with other molecules and the

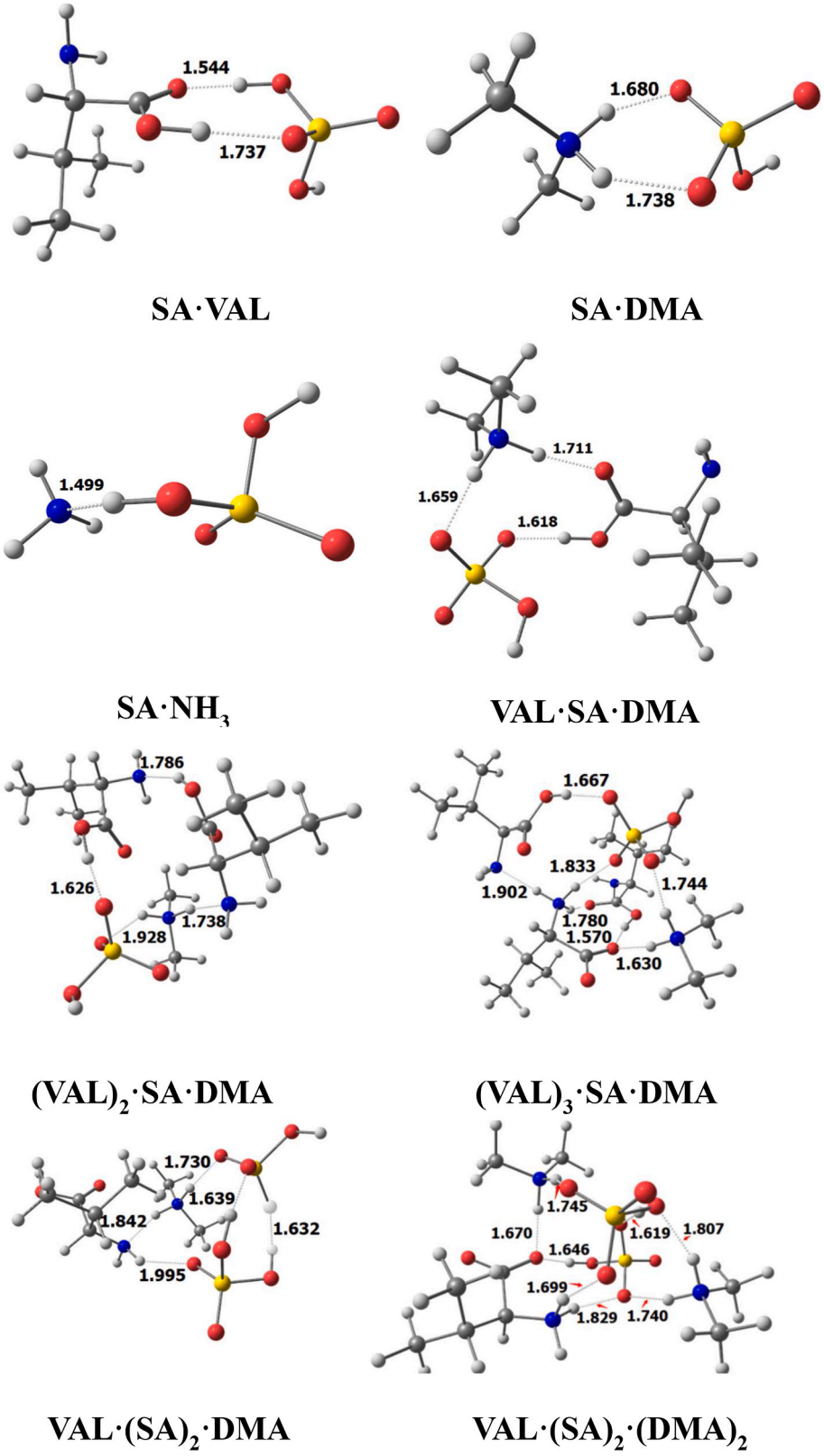

Fig. 1. Some representative molecular geometries of the global minima of $(SA)_x(DMA)_y(VAL)_z(0 \leq x, y, z \leq 3)$ obtained at the ωB97XD/6-31++G(d, p) level of theory and basis set. The unit of molecular hydrogen bond distance is angstroms. (The red balls represent oxygen atoms, blue is for nitrogen atoms, yellow is for sulfuric atoms, and white is for hydrogen atoms.). (For interpretation of the references to color in this figure legend, the reader is referred to the Web version of this article.)

structure becomes more complex and stable as well.

In general, amino acids can participate in the nucleation along with different directions according to different functional groups when predicting their participation in NPF.

3.2. Thermodynamics analysis of clusters

Table 1 illustrates the relative binding energy changes (ΔE_{0K}), intermolecular enthalpies ($\Delta H_{278.15\ K}$) and Gibbs free energy changes ($\Delta G_{278.15\ K}$) of the lowest energy conformer dimers and some trimers clusters of $(SA)_x(DMA)_y(VAL)_z$($0 \leq x, y, z \leq 3$) system at the ωB97XD/6-31++G(d, p) theory level and basis set. These three parameters are important features for studying the stability of aerosol nucleation. A negative relative binding energy indicates that the reaction is exothermic and the system tends to be stable and a negative value of Gibbs free energy indicates that the reaction can proceed spontaneously. ΔG is obtained by the reaction path of adding a single molecule, as shown in equation (4), and ΔE and ΔH are calculated in the same way.

$$\text{path: } \Delta G = G_{(SA)x\cdot(DMA)y\cdot(VAL)z} - x\ G_{(SA)} - y\ G_{(DMA)} - z\ G_{(VAL)} \quad (4)$$

The ΔG value of the cluster given in Table 1 is all negative. It can be seen that the ΔG value of $(VAL)_1\cdot(SA)_1$ is lower than that of $(SA)_1\cdot(SA)_1$ cluster (-9.16 kcal mol^{-1} vs. -5.88 kcal mol^{-1}), which indicates that SA is easier to combine with VAL rather than SA itself. In binary clusters involved VAL, the ΔG value of SA-VAL cluster is lower than that of DMA-VAL cluster (-9.16 kcal mol-1 vs. -3.58 kcal mol-1), which could be explained by the strong hydrogen bonded molecular interactions between SA and VAL, for VAL is a weak acid compared with SA. The ΔG value of the dimer $(VAL)_1\cdot(SA)_1$ is less negative than that of $(SA)_1\cdot(DMA)_1$ (-9.16 kcal mol^{-1} vs -15.19 kcal mol^{-1}), which may be due to the strong acid-base stabilization in SA-DMA clusters, meanwhile, proton transfer occurs in SA-DMA cluster, but no proton transfer occurs in SA-VAL cluster in the structural analysis, which could also explain the result. However, the ΔG value of the ternary SA-DMA-VAL clusters are more negative as VAL continuously added to the acid-base dimer $(SA)_1\cdot(DMA)_1$ cluster. From a thermodynamic point of view, the addition of VAL is favorable for stabilizing SA-DMA clusters.

Table 2 lists the Gibbs free energy of binary SA-DMA cluster and ternary SA-DMA-VAL cluster at the same total number molecules and the same SA number molecules, just making DMA replaced by VAL correspondingly. The ternary clusters ΔG value is less than that of binary clusters when the number of SA molecules is 1, which indicates that the stability of ternary SA-DMA-VAL is better than that of binary SA-DMA

Table 1
The thermodynamic parameters (kcal mol^{-1}) of binary clusters $(VAL)_1\cdot(SA)_1$, $(SA)_1\cdot(DMA)_1$, $(VAL)_1\cdot(DMA)_1$ and ternary clusters when VAL is sequentially added to $(DMA)_1\cdot(SA)_1$, $(DMA)_2\cdot(SA)_2$, $(DMA)_3\cdot(SA)_3$. The energy is calculated at the theory level and basis set of ωB97XD/6-31++G (d, p).

Reactions	△E (0 K)	△H (278.15 K)	△G (278.15 K)
VAL+DMA→$(VAL)_1\cdot(DMA)_1$	−13.86	−13.92	−3.58
SA+SA→$(SA)_2$	−17.96	−18.20	−5.88
VAL+SA→$(VAL)_1\cdot(SA)_1$	−19.37	−19.37	−9.16
SA+DMA→$(SA)_1\cdot(DMA)_1$	−23.81	−23.60	−15.19
VAL+DMA+SA→ $(VAL)_1\cdot(DMA)_1\cdot(SA)_1$	−46.50	−46.20	−25.64
2VAL+DMA+SA→ $(VAL)_2\cdot(DMA)_1\cdot(SA)_1$	−69.61	−69.80	−34.43
3VAL+DMA+SA→ $(VAL)_3\cdot(DMA)_1\cdot(SA)_1$	−91.01	−91.59	−43.12
2VAL+2DMA+2SA→ $(VAL)_2\cdot(DMA)_2\cdot(SA)_2$	−117.59	−117.77	−60.45
3VAL+2DMA+2SA→ $(VAL)_3\cdot(DMA)_2\cdot(SA)_2$	−143.35	−143.29	−75.43
3VAL+3DMA+3SA→ $(VAL)_3\cdot(DMA)_3\cdot(SA)_3$	−220.92	−222.62	−123.33

Table 2
The Gibbs free energy (kcal mol^{-1}) of SA-DMA and SA-DMA-Val clusters sharing the same number of molecules. The energy is calculated at the theory level and basis set of ωB97XD/6-31++G (d, p).

Cluster	ΔG	Clusters	ΔG
$(SA)_1\cdot(DMA)_2$	−18.36	$(SA)_1\cdot(DMA)_1\cdot(Val)_1$	−24.16
$(SA)_1\cdot(DMA)_3$	−22.00	$(SA)_1\cdot(DMA)_1\cdot(Val)_2$	−31.88
		$(SA)_1\cdot(DMA)_2\cdot(Val)_1$	−33.51
$(SA)_2\cdot(DMA)_2$	−49.74	$(SA)_2\cdot(DMA)_1\cdot(Val)_1$	−37.14
$(SA)_2\cdot(DMA)_3$	−59.45	$(SA)_2\cdot(DMA)_1\cdot(Val)_2$	−51.45
		$(SA)_2\cdot(DMA)_2\cdot(Val)_1$	−54.44
$(SA)_3\cdot(DMA)_2$	−65.96	$(SA)_3\cdot(DMA)_1\cdot(Val)_1$	−59.91
$(SA)_3\cdot(DMA)_3$	−85.31	$(SA)_3\cdot(DMA)_1\cdot(Val)_2$	−67.33
		$(SA)_3\cdot(DMA)_2\cdot(Val)_1$	−80.79

and the synergistic effect of VAL on acid and base makes ternary clusters easier to form. However, the Gibbs free energy of acid-base binary combination is smaller and the clusters tend to be more stable than the ternary SA-DMA-VAL clusters as the number of SA increasing. This may benefit from the strong binding ability of strong acids and strong bases of SA and DMA.

As shown in Table S4, when VAL molecular is made to replace SA molecular in the SA-DMA system, the Gibbs free energy of ternary system SA-DMA-VAL is always higher than that of binary system SA-DMA, and the values of energy difference vary greatly, which indicates that VAL is more inclined to replace DMA acting as a base in the nucleation of cluster SA-DMA rather than replacing SA acting as an acid when sharing the same number of molecules.

Fig. 2 demonstrates the Gibbs free energy of different size of SA-DMA-VAL clusters, Fig. 2a shows the Gibbs free energy of binary clusters $(VAL)_x(DMA)_y$ ($0 \leq x, y \leq 3$) when the number of SA is zero, and b, c, and d show the heat maps of Gibbs free energy formed by the ternary $(SA)_x(DMA)_y(VAL)_z$ ($1 \leq x, y, z \leq 3$) when the number of SA molecules in the cluster is 1, 2, and 3, respectively.

The Gibbs free energy of the cluster tends to gradually decrease with the increasing number of SA, DMA, and VAL molecules. The Gibbs free energy changes significantly when the cluster contains both SA and DMA compared with the clusters containing no SA, which may be related to the proton transfer between acid and base. Meanwhile, protons transfer occurs in VAL as VAL is added to the cluster, which may further enhance the stability of the clusters. The smallest Gibbs free energy existing in cluster $(SA)_x(DMA)_y(VAL)_z$ ($0 \leq x, y, z \leq 3$) reaches -123 kcal mol^{-1}. It can be seen from all four figures that the Gibbs free energy decreases rapidly along the diagonal, thus, it can be inferred that the large-sized nucleation may grow along the diagonal direction to detectable particle size.

3.3. Evaporation rates

Quantum chemical calculation was used to calculate the thermodynamic parameters of different clusters to better understand new particle formation. These thermodynamic parameters reflect the relative stability of the cluster, however, they are not sufficient to evaluate the growth of clusters from small to large in the real atmospheric environment. The influence of kinetics should also be considered in addition to the thermodynamics analysis (Ortega et al., 2011). It is generally believed that clusters of a given size are formed by collisions of two smaller clusters as well as the evaporation of larger clusters, and they move to another size when they collide or evaporate with other clusters. Therefore, it is necessary to study the collision and evaporation rate to reveal the formation and stability of the cluster.

The evaporation rates of $(SA)_x(DMA)_y(VAL)_z$ ($0 \leq x, y, z \leq 3$) ternary clusters containing different numbers of SA molecules of VAL-DMA grid at 278.15K at ωB97XD/6-31++G(d, p) theory level and basis set are shown in Fig. 3. When paying attention to the number of SA molecules and DMA molecules in these four pictures, it can be found that the

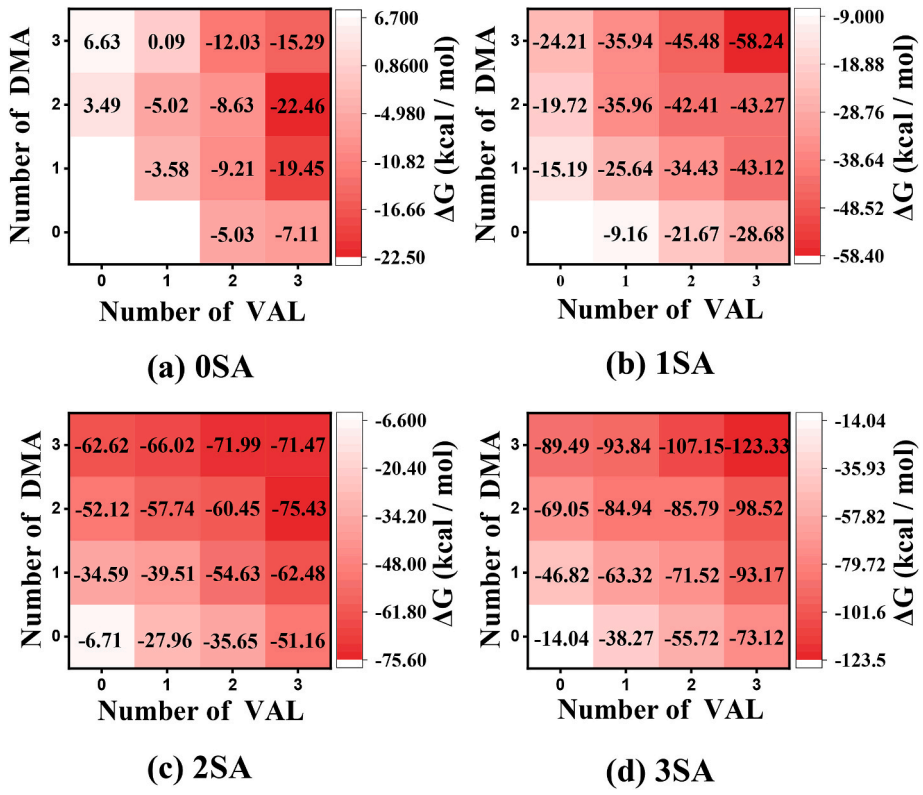

Fig. 2. The Gibbs free energies changes for $(SA)_x(DMA)_y(VAL)_z$ ($0 \leq x, y, z \leq 3$) clusters on different numbers of SA molecules at the ωB97XD/6-31++G(d, p) theory level and basis set and at 298.15 K at 1 atm. Where, a, b, c, d corresponds to the number of SA molecules equals 0, 1, 2, 3 respectively.

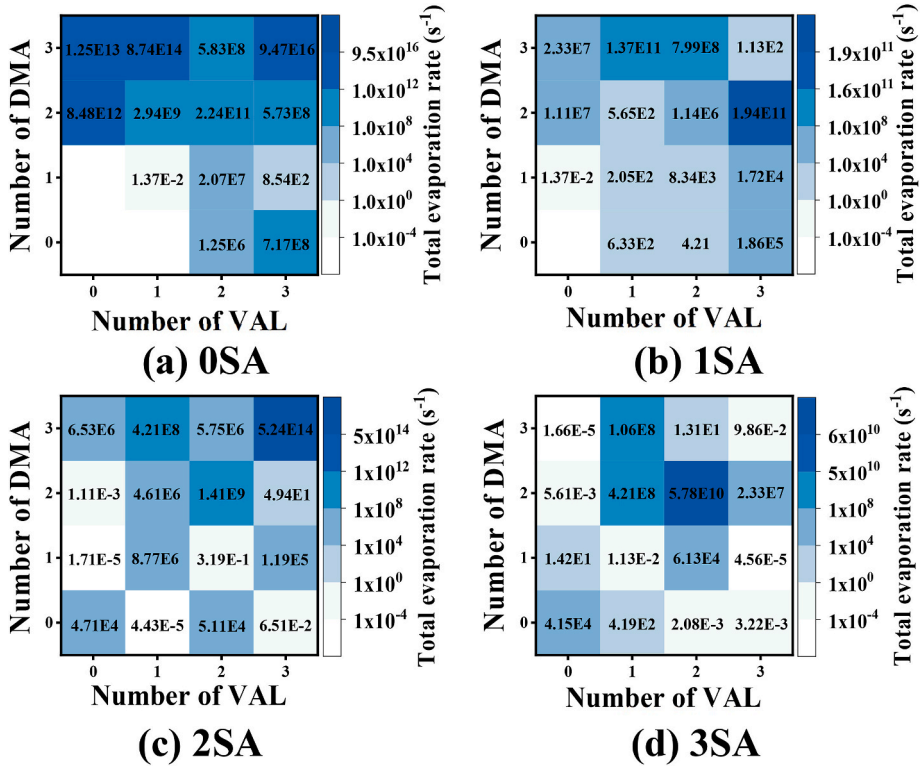

Fig. 3. Evaporation rates for $(SA)_x(DMA)_y(VAL)_z$ ($0 \leq x, y, z \leq 3$) on the VAL-DMA grid at 278.15 K and at ωB97XD/6-31++G(d, p) theory level and basis set. Where figure a, b, c, d represent the number of SA molecules as 0, 1, 2, and 3, respectively.

evaporation rate of the cluster is generally very large when the number of SA molecules is less than that of DMA molecules compared with the case where the number of SA molecules is greater than or equal to the number of DMA molecules. This may be explained by the steric hindrance, which may become the main element that affects the stability of the cluster when the number of DMA is greater than or equal to SA. Therefore, it is generally believed that a cluster containing more number of DMA molecules than SA molecules is not thermodynamically stable.

As shown in Fig. 3 c, the cluster contains 2 molecules of SA. It can be seen that when the number of DMA is greater than 2, the minimum evaporation rate of the cluster is 10^6 orders, the largest is 10^{14} orders, however, the evaporation rate of those clusters containing less than or equal to 2 molecules of DMA is mostly below 10^5 in addition to three unique values, and the lowest evaporation rate can even reach 10^{-5}. When there is no SA molecule in the cluster, as shown in Fig. 3 a, the evaporation rate of the vast majority of clusters is above 10^6, which is much larger than the other three cases containing SA molecule. The above results reveal that SA molecules can enhance the nucleation ability of VAL-DMA.

Table S2 lists the evaporation rates of acid-base binary clusters $(SA)_x(DMA)_y$ ($0\leq x, y \leq 3$) and ternary clusters $(SA)_x(DMA)_y(VAL)_z$ ($0\leq x, y, z \leq 3$) on different evaporation paths. For acid-base binary system $(SA)_x(DMA)_y$ ($0\leq x, y \leq 3$), when the number of SA and DMA molecules is not equal, the main evaporation path is that the monomers with a larger number of molecules in SA and DMA tend to evaporate from the cluster, in contrast, when the number of SA and DMA is equal, DMA is more inclined to evaporate from clusters. However, cluster $(SA)_2{\cdot}(DMA)_3$ is preferred to evaporate the dimer $(DMA)_2$, which may be an explanation by that the Gibbs free energy of $(SA)_2{\cdot}(DMA)$ is lower than that of $(SA)_2{\cdot}(DMA)_2$ and thus $(SA)_2{\cdot}(DMA)_1$ has a more stable structure. When SA-DMA-VAL is included in the cluster simultaneously, the main path in all cases is that DMA monomer evaporate from the cluster, which illustrates the strong stability of SA-DMA indirectly(Yao et al., 2018).

3.4. Comparison with results from CLOUD experiments

A report from the CLOUD experiment at CERN by João Almeida et al. (Kirkby et al., 2011) showed observations of SA and amine/ammonia nucleation at atmospheric against SA concentration at 278 K and 38% relative humidity (RH), which was considered representative of a wide range of boundary layer conditions(Almeida et al., 2013; Kirkby et al., 2011). The results of the CLOUD data demonstrated that under conditions (0.1 p.p.t.v. DMA and 2–250 p.p.t.v. NH3), the J (the formation rates of the clusters obtained by dynamics simulation based on Atmospheric Cluster Dynamics Code) of ammonia ternary (SA-NH_3-W) is $10^{-2}\ cm^{-3}s^{-1}$ when the concentration of SA is about $10^7\ cm^{-3}$, and the J is less than $10^1\ cm^{-3}s^{-1}$ when the concentration of SA is about $10^8\ cm^{-3}$. However, under conditions (5-140 p.p.t.v. DMA), the J of amine ternary (SA-DMA-W) is $10^{-2}\ cm^{-3}s^{-1}$ when the concentration of SA is about $10^6\ cm^{-3}$, and the J is $10^2\ cm^{-3}s^{-1}$ when the concentration of SA is about $10^7\ cm^{-3}$.

Fig. 4 shows the theoretical nucleation expectations of amine ternary (SA-DMA-VAL) simulated by Atmospheric Cluster Dynamics Code model (ACDC) at 278 K. Here, the concentrations of VAL and DMA were set to 100 ppt and 10 ppt respectively, while SA concentration ranged from 10^5 to $10^9\ cm^{-3}$. Comparing with the atmospheric CLOUD data at the same temperature, the nucleation rate of SA-DMA-VAL is higher than that of SA-NH_3-W, but lower than that of SA-DMA-W, indicating that the nucleation rate of SA-DMA-VAL is between amine ternary and ammonia ternary. Besides, the slope of the straight line of SA-DMA-VAL nucleation rate is lower than that of SA-DMA-VAL, the growth rate of J value against SA would be much lower with the increment of SA concentration than SA-DMA-W. The formation rates of SA-DMA from ACDC simulation are higher than the CLOUD measurements, which might due to the smaller simulation size (three SA and three DMA), thus, the formation rates of SA-DMA are expected to overestimate the result from the CLOUD experiments. The phenomenon is consistent with the previous studies.

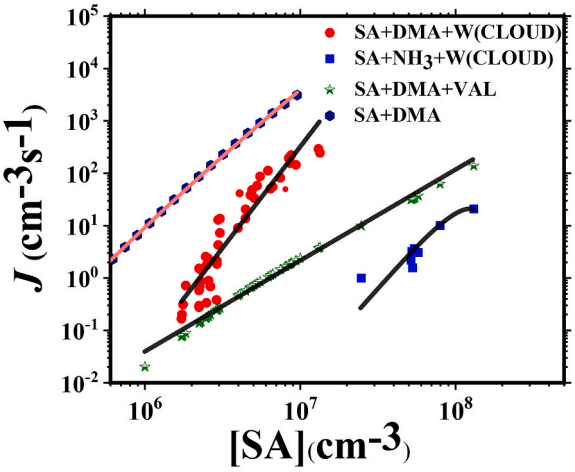

Fig. 4. Plot of formation rates J ($cm^{-3}s^{-1}$) of ternary cluster SA-DMA-W, SA-NH_3-W and SA-DMA-VAL against SA concentration. The red dots represent the formation rate of SA-DMA-W, green stars represent the formation rate of SA-DMA-VAL, the dark hexagons represent the formation rate of SA-DMA, and the blue squares represent the formation rate of SA-NH_3-W. The observed formation rates of cluster SA-NH_3-W and SA-DMA-W are all from the CLOUD in boundary layer conditions. The formation rate of cluster SA-DMA-VAL and cluster SA-DMA were simulated at ωB97XD/6-31++G (d, p) theory level. All observations and simulations were performed at 278 K. (For interpretation of the references to color in this figure legend, the reader is referred to the Web version of this article.)

In clusters of larger molecules, the functional groups of amino acids that could participate in the reaction are in a saturated state, and there are no other binding sites, which increases the steric hindrance effect and hinders the further proximity and collision of other molecules (SA&DMA), which inhibits the further growth of the ternary cluster in the initial nucleation stage. The growth in the initial stage may be dominated by SA and DMA acid-base nucleation mechanisms.

Previous studies have shown that the thermodynamic parameters of clusters are affected by temperature, so the evaporation rate and formation rate of clusters are temperature-dependent parameters (Li et al., 2019; Tiszenkel et al., 2019). Research by N. Bork et al. reveals that the difference in the formation rate of clusters at different temperatures is relatively large(Bork et al., 2014). In view of the effect of temperature, we discuss the influence of temperature on the nucleation rate.

Fig. 5 shows the relation between the formation rate of the ternary system $(SA)_x(DMA)_y(VAL)_z$ ($0\leq x, y, z \leq 3$) and the SA molecular concentration at three different temperatures. For the same cluster size and the same concentration of nucleating substances, when the temperature is 298K, 278K, and 258K, the formation rate change ranges from 10^{-6}-10^1 $cm^{-3}s^{-1}$, 10^{-5}-10^2 $cm^{-3}s^{-1}$, and 10^{-3}-10^3 $cm^{-3}s^{-1}$ respectively. The result indicates that the influence of temperature on the formation rate is negatively correlated, the lower the temperature, the more favorable for the formation of new particles.

In order to better understand the role of VAL in the nucleation of SA-DMA-VAL system, the main formation pathways of pure SA-DMA and VAL-containing SA-DMA-VAL system traced by ACDC is shown in Fig. 6. The condition is consistent with the simulation where [SA] = 3e6 cm^{-3}, [DMA] = 10 ppt, [VAL] = 100 ppt.

It can be seen from Fig. 6, the growth path of pure SA-DMA clusters shows the same tendency with the previous studies, the cluster $(SA)_1(DMA)_1$ is the first step (Bork et al., 2014; Olenius et al., 2013). SA-DMA grows along diagonal to form $(SA)_2(DMA)_2$ or collides with SA monomer to form $(SA)_2$DMA and then collides with DMA to form

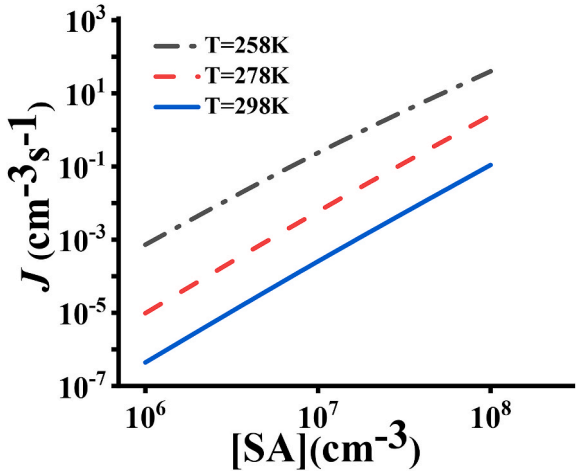

Fig. 5. The cluster formation rate J ($cm^{-3}s^{-1}$) against SA concentration for system $(SA)_x(DMA)_y(VAL)_z$ ($0 \leq x, y, z \leq 3$) on different temperatures at ωB97XD/6-31++G(d, p) theory level and basis set. The black double-dotted line represents the case of T = 258K, the red dotted line represents the case of T = 278K and the blue solid line represents the case of T = 298K. (For interpretation of the references to color in this figure legend, the reader is referred to the Web version of this article.)

$(SA)_2(DMA)_2$ at last. The pathways of cluster $(SA)_2(DMA)_2$ to $(SA)_3(DMA)_3$ show the same ways with the cluster (SA)(DMA) to $(SA)_2(DMA)_2$. However, for the formation routes of VAL-containing system, as shown in yellow lines, the (SA)(VAL) is the first step in the initial nucleation stage, rather than (SA)(DMA). Though (SA)(DMA) is rather more stable than (SA)(VAL) for base stabilization mechanism. Then (SA)(VAL) collides with VAL monomer to form $(SA)(VAL)_2$, after that, there are two paths to form $(SA)_3(VAL)_2(DMA)_3$ from the cluster $(SA)(VAL)_2$: (1) $(SA)(VAL)_2 + DMA \rightarrow (SA)(VAL)_2(DMA)$, $(SA)(VAL)_2(DMA)+(SA)_2(DMA)_2 \rightarrow (SA)_3(VAL)_2(DMA)_3$ (2) $(SA)(VAL)_2+(SA)_2(DMA)_3 \rightarrow (SA)_3(VAL)_2(DMA)_3$. The two paths shows that the collision between cluster and cluster to form bigger cluster is the main pathway, rather than cluster and monomers or dimers, which differs from SA and DMA. It is obvious that VAL plays an important role in the SA-DMA-VAL system, it acts as a direct participant in the cluster formation and changes the formation pathways mode of pure SA-DMA.

4. Conclusion

Large amounts of valine (VAL) were found in droplets and gas-phase aerosols in cities and suburbs. The effect and role of VAL in the formation of $(SA)_x(DMA)_y(VAL)_z$ ($0 \leq x, y, z \leq 3$) molecular clusters in atmospheres have been investigated in this study. The low-energy configurations of the clusters were optimized to get global minimum structures and the thermodynamic properties were calculated. By structural analysis, the number of hydrogen bonds in the cluster increases as the cluster size increasing, and proton transfer could be more as well, suggesting that the cluster gradually tends to be stable, and VAL could combine SA molecular and DMA molecular from both the amino and carboxyl group directions. The thermodynamic energy ($\Delta G_{278.15\ K}$) of the cluster drops rapidly along with the diagonal distribution, thus the clusters near the diagonal could be considered relatively stable and it could be inferred that the growth of clusters may grow along the diagonal. The Gibbs free energy of the ternary cluster structure is lower than that of the binary cluster structure with the addition of VAL, meanwhile, the Gibbs free energy gradually decreases with the increasing of clusters size, indicating that the cluster has the potential to continue to grow. The evaporation rates and formation rates of clusters obtained by the simulation of Atmospheric Cluster Dynamics Code (ACDC) at 278 K show that ternary clusters containing SA molecules have lower evaporation rates than that of clusters containing only VAL and DMA, which indicates that SA has a synergistic effect with binary clusters. The dibasic acid-base system tends to evaporate molecules with more numbers, while the ternary cluster tends to evaporate the VAL monomer. Compared with the observation results from the CLOUD experiment under boundary layer conditions, the nucleation rate of SA-DMA-VAL system is lower than that of SA-DMA-W system but higher than that of SA-NH3-W system, and the nucleation ability of ternary SA-DMA-VAL system is negatively related to temperature, it can be speculated that SA-DMA-VAL is more likely to nucleate at low temperatures. In summary, our study may provide an important theoretical guiding significance for the nucleation of acid-base system involving VAL in initial formation and growth process.

CRediT authorship contribution statement

Ying Liu: Conceptualization, Methodology, Data curation, Writing – original draft, Writing – review & editing. **Yi-Rong Liu:** Methodology, Validation, Formal analysis, Writing – review & editing. **Ya-Juan Feng:** Software, Investigation, Visualization. **Teng Huang:** Resources. **Shuai**

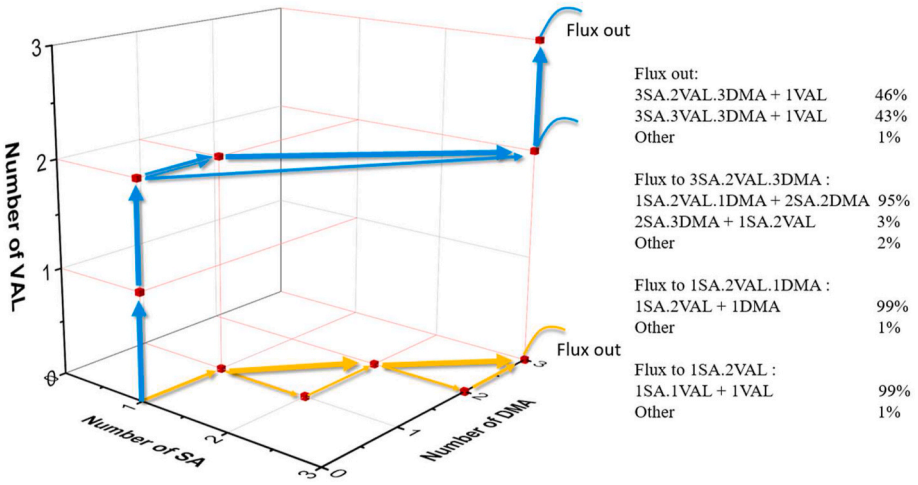

Fig. 6. The main formation routes of pure SA-DMA and VAL-containing SA-DMA-VAL system simulated by ACDC at the condition where [SA] = 3e6 cm^{-3}, [DMA] = 10 ppt, [VAL] = 100 ppt. The blue lines represent the formation route of SA-DMA and the yellow lines represent the formation route of SA-DMA-VAL. (For interpretation of the references to color in this figure legend, the reader is referred to the Web version of this article.)

Jiang: Formal analysis, Data curation. **Zi-Hang Wang:** Writing – review & editing. **Hui Cao:** Visualization. **Wei Huang:** Methodology, Software, Supervision, Project administration, Funding acquisition.

Declaration of competing interest

The authors declare that they have no known competing financial interests or personal relationships that could have appeared to influence the work reported in this paper.

Acknowledgments

This work was supported by the National Key Research and Development Program (Grant No. 2016YFC0202203), the National Natural Science Foundation of China (Grant No. 41877305, 41605099, 41705097, 41705111, 41775112 and 41527808), the National Science Fund for Distinguished Young Scholars (Grant No. 41725019), the Key Research Program of Frontier Science, CAS (Grant No. QYZDB-SSW-DQC031), the National Research Program for Key Issues in Air Pollution Control (DQGG0103), the Fundamental Research Funds for the Central Universities of China (Grant No. WK2100000008).

Appendix A. Supplementary data

Supplementary data to this article can be found online at https://doi.org/10.1016/j.atmosenv.2021.118373.

References

Almeida, J., Schobesberger, S., Kürten, A., Ortega, I.K., Kupiainen-Määttä, O., Praplan, A. P., Adamov, A., Amorim, A., Bianchi, F., Breitenlechner, M., David, A., Dommen, J., Donahue, N.M., Downard, A., Dunne, E., Duplissy, J., Ehrhart, S., Flagan, R.C., Franchin, A., Guida, R., Hakala, J., Hansel, A., Heinritzi, M., Henschel, H., Jokinen, T., Junninen, H., Kajos, M., Kangasluoma, J., Keskinen, H., Kupc, A., Kurtén, T., Kvashin, A.N., Laaksonen, A., Lehtipalo, K., Leiminger, M., Leppä, J., Loukonen, V., Makhmutov, V., Mathot, S., McGrath, M.J., Nieminen, T., Olenius, T., Onnela, A., Petäjä, T., Riccobono, F., Riipinen, I., Rissanen, M., Rondo, L., Ruuskanen, T., Santos, F.D., Sarnela, N., Schallhart, S., Schnitzhofer, R., Seinfeld, J. H., Simon, M., Sipilä, M., Stozhkov, Y., Stratmann, F., Tomé, A., Tröstl, J., Tsagkogeorgas, G., Vaattovaara, P., Viisanen, Y., Virtanen, A., Vrtala, A., Wagner, P. E., Weingartner, E., Wex, H., Williamson, C., Wimmer, D., Ye, P., Yli-Juuti, T., Carslaw, K.S., Kulmala, M., Curtius, J., Baltensperger, U., Worsnop, D.R., Vehkamäki, H., Kirkby, J., 2013. Molecular understanding of sulphuric acid–amine particle nucleation in the atmosphere. Nature 502, 359–363.

Arquero, K.D., Gerber, R.B., Finlayson-Pitts, B.J., 2017. The role of oxalic acid in new particle formation from methanesulfonic acid, methylamine, and water. Environ. Sci. Technol. 51, 2124–2130.

Asmi, E., Kondratyev, V., Brus, D., Laurila, T., Lihavainen, H., Backman, J., Vakkari, V., Aurela, M., Hatakka, J., Viisanen, Y., Uttal, T., Ivakhov, V., Makshtas, A., 2016. Aerosol size distribution seasonal characteristics measured in Tiksi, Russian Arctic. Atmos. Chem. Phys. 16, 1271–1287.

Barbaro, E., Zangrando, R., Moret, I., Barbante, C., Cescon, P., Gambaro, A., 2011. Free amino acids in atmospheric particulate matter of Venice, Italy. Atmos. Environ. 45, 5050–5057.

Berndt, T., Böge, O., Stratmann, F., Heintzenberg, J., Kulmala, M., 2005. Rapid formation of sulfuric acid particles at near-atmospheric conditions. Science 307, 698.

Bork, N., Elm, J., Olenius, T., Vehkamäki, H., 2014. Methane sulfonic acid-enhanced formation of molecular clusters of sulfuric acid and dimethyl amine. Atmos. Chem. Phys. 14, 12023–12030.

Boy, M., Kulmala, M., Ruuskanen, T.M., Pihlatie, M., Reissell, A., Aalto, P.P., Keronen, P., Dal Maso, M., Hellen, H., Hakola, H., Jansson, R., Hanke, M., Arnold, F., 2005. Sulphuric acid closure and contribution to nucleation mode particle growth. Atmos. Chem. Phys. 5, 863–878.

Chan, M.N., Choi, M.Y., Ng, N.L., Chan, C.K., 2005. Hygroscopicity of water-soluble organic compounds in atmospheric Aerosols: amino acids and biomass burning derived organic species. Environ. Sci. Technol. 39, 1555–1562.

Charlson, R.J., Schwartz, S.E., Hales, J.M., Cess, R.D., Coakley, J.A., Hansen, J.E., Hofmann, D.J., 1992a. Climate forcing by anthropogenic aerosols. Science 255, 423.

Charlson, R.J., Schwartz, S.E., Hales, J.M., Cess, R.D., Coakley Jr., J.A., Hansen, J.E., Hofmann, D.J., 1992b. Climate forcing by anthropogenic aerosols. Science 255, 423–430.

Charlson, R.J., Seinfeld, J.H., Nenes, A., Kulmala, M., Laaksonen, A., Facchini, M.C., 2001. Atmospheric science: reshaping the theory of cloud formation. Science 292, 2025–2026.

Cornell, S.E., 2011. Atmospheric nitrogen deposition: revisiting the question of the importance of the organic component. Environ. Pollut. 159, 2214–2222.

Cornell, S.E., Jickells, T.D., Cape, J.N., Rowland, A.P., Duce, R.A., 2003. Organic nitrogen deposition on land and coastal environments: a review of methods and data. Atmos. Environ. 37, 2173–2191.

De Haan, D.O., Corrigan, A.L., Smith, K.W., Stroik, D.R., Turley, J.J., Lee, F.E., Tolbert, M.A., Jimenez, J.L., Cordova, K.E., Ferrell, G.R., 2009. Secondary organic aerosol-forming reactions of glyoxal with amino acids. Environ. Sci. Technol. 43, 2818–2824.

Di Filippo, P., Pomata, D., Riccardi, C., Buiarelli, F., Gallo, V., Quaranta, A., 2014. Free and combined amino acids in size-segregated atmospheric aerosol samples. Atmos. Environ. 98, 179–189.

Ehn, M., Thornton, J.A., Kleist, E., Sipilä, M., Junninen, H., Pullinen, I., Springer, M., Rubach, F., Tillmann, R., Lee, B., Lopez-Hilfiker, F., Andres, S., Acir, I.-H., Rissanen, M., Jokinen, T., Schobesberger, S., Kangasluoma, J., Kontkanen, J., Nieminen, T., Kurtén, T., Nielsen, L.B., Jørgensen, S., Kjaergaard, H.G., Canagaratna, M., Maso, M.D., Berndt, T., Petäjä, T., Wahner, A., Kerminen, V.-M., Kulmala, M., Worsnop, D.R., Wildt, J., Mentel, T.F., 2014. A large source of low-volatility secondary organic aerosol. Nature 506, 476–479.

Elm, J., Bilde, M., Mikkelsen, K.V., 2013a. Assessment of binding energies of atmospherically relevant clusters. Phys. Chem. Chem. Phys. 15, 16442–16445.

Elm, J., Fard, M., Bilde, M., Mikkelsen, K.V., 2013b. Interaction of Glycine with common atmospheric nucleation precursors. J. Phys. Chem. A 117, 12990–12997.

Elm, J., Jen, C.N., Kurtén, T., Vehkamäki, H., 2016. Strong hydrogen bonded molecular interactions between atmospheric diamines and sulfuric acid. J. Phys. Chem. A 120, 3693–3700.

Feltracco, M., Barbaro, E., Kirchgeorg, T., Spolaor, A., Turetta, C., Zangrando, R., Barbante, C., Gambaro, A., 2019. Free and combined L- and D-amino acids in Arctic aerosol. Chemosphere 220, 412–421.

Frisch, M., T, G., Schlegel, H., Scuseria, G., Robb, M., Cheeseman, J., Scalmani, G., Barone, V., Mennucci, B., Petersson, G., 2013. Gaussian 09, Revision D. 01, 2013, Gaussian. Gaussian Inc, Wallingford CT, 2013.

Ge, X., Wexler, A.S., Clegg, S.L., 2011. Atmospheric amines – Part I. A review. Atmos. Environ. 45, 524–546.

Ge, P., Luo, G., Luo, Y., Huang, W., Xie, H., Chen, J., Qu, J., 2018. Molecular understanding of the interaction of amino acids with sulfuric acid in the presence of water and the atmospheric implication. Chemosphere 210, 215–223.

Haywood, J.M., Ramaswamy, V., 1998. Global sensitivity studies of the direct radiative forcing due to anthropogenic sulfate and black carbon aerosols. J. Geophys. Res. Atmos. 103, 6043–6058.

Hostaš, J., Řezáč, J., Hobza, P., 2013. On the performance of the semiempirical quantum mechanical PM6 and PM7 methods for noncovalent interactions. Chem. Phys. Lett. 568–569, 161–166.

Hou, X.-F., Yan, L.-L., Huang, T., Hong, Y., Miao, S.-K., Peng, X.-Q., Liu, Y.-R., Huang, W., 2016. A density functional theory study on structures, stabilities, and electronic and magnetic properties of AunC (n=1–9) clusters. Chem. Phys. 472, 50–60.

Huang, W., Pal, R., Wang, L.-M., Zeng, X.C., Wang, L.-S., 2010. Isomer identification and resolution in small gold clusters. J. Chem. Phys. 132, 054305.

Jiang, S., Liu, Y.-R., Huang, T., Wen, H., Xu, K.-M., Zhao, W.-X., Zhang, W.-J., Huang, W., 2014. Study of Cl−(H2O)n (n = 1–4) using basin-hopping method coupled with density functional theory. J. Comput. Chem. 35, 159–165.

Kecorius, S., Vogl, T., Paasonen, P., Lampilahti, J., Rothenberg, D., Wex, H., Zeppenfeld, S., van Pinxteren, M., Hartmann, M., Henning, S., Gong, X., Welti, A., Kulmala, M., Stratmann, F., Herrmann, H., Wiedensohler, A., 2019. New particle formation and its effect on cloud condensation nuclei abundance in the summer Arctic: a case study in the Fram Strait and Barents Sea. Atmos. Chem. Phys. 19, 14339–14364.

Kerminen, V.M., Petäjä, T., Manninen, H.E., Paasonen, P., Nieminen, T., Sipilä, M., Junninen, H., Ehn, M., Gagné, S., Laakso, L., Riipinen, I., Vehkamäki, H., Kurten, T., Ortega, I.K., Dal Maso, M., Brus, D., Hyvärinen, A., Lihavainen, H., Leppä, J., Lehtinen, K.E.J., Mirme, A., Mirme, S., Hõrrak, U., Berndt, T., Stratmann, F., Birmili, W., Wiedensohler, A., Metzger, A., Dommen, J., Baltensperger, U., Kiendler-Scharr, A., Mentel, T.F., Wildt, J., Winkler, P.M., Wagner, P.E., Petzold, A., Minikin, A., Plass-Dülmer, C., Pöschl, U., Laaksonen, A., Kulmala, M., 2010. Atmospheric nucleation: highlights of the EUCAARI project and future directions. Atmos. Chem. Phys. 10, 10829–10848.

Kerminen, V.-M., Chen, X., Vakkari, V., Petäjä, T., Kulmala, M., Bianchi, F., 2018. Atmospheric new particle formation and growth: review of field observations. Environ. Res. Lett. 13, 103003.

Kirkby, J., Curtius, J., Almeida, J., Dunne, E., Duplissy, J., Ehrhart, S., Franchin, A., Gagné, S., Ickes, L., Kürten, A., Kupc, A., Metzger, A., Riccobono, F., Rondo, L., Schobesberger, S., Tsagkogeorgas, G., Wimmer, D., Amorim, A., Bianchi, F., Breitenlechner, M., David, A., Dommen, J., Downard, A., Ehn, M., Flagan, R.C., Haider, S., Hansel, A., Hauser, D., Jud, W., Junninen, H., Kreissl, F., Kvashin, A., Laaksonen, A., Lehtipalo, K., Lima, J., Lovejoy, E.R., Makhmutov, V., Mathot, S., Mikkilä, J., Minginette, P., Mogo, S., Nieminen, T., Onnela, A., Pereira, P., Petäjä, T., Schnitzhofer, R., Seinfeld, J.H., Sipilä, M., Stozhkov, Y., Stratmann, F., Tomé, A., Vanhanen, J., Viisanen, Y., Vrtala, A., Wagner, P.E., Walther, H., Weingartner, E., Wex, H., Winkler, P.M., Carslaw, K.S., Worsnop, D.R., Baltensperger, U., Kulmala, M., 2011. Role of sulphuric acid, ammonia and galactic cosmic rays in atmospheric aerosol nucleation. Nature 476, 429–433.

Kollman, P.A., Allen, L.C., 1972. Theory of the hydrogen bond. Chem. Rev. 72, 283–303.

Kristensson, A., Rosenørn, T., Bilde, M., 2010. Cloud droplet activation of amino acid aerosol particles. J. Phys. Chem. A 114, 379–386.

Kuang, C., McMurry, P.H., McCormick, A.V., Eisele, F.L., 2008. Dependence of nucleation rates on sulfuric acid vapor concentration in diverse atmospheric locations. J. Geophys. Res.: Atmospheres 113.

Kulmala, M., 2003. How particles nucleate and grow. Science 302, 1000.

Kulmala, M., Pirjola, L., Mäkelä, J.M., 2000. Stable sulphate clusters as a source of new atmospheric particles. Nature 404, 66–69.
Kulmala, M., Vehkamäki, H., Petäjä, T., Dal Maso, M., Lauri, A., Kerminen, V.M., Birmili, W., McMurry, P.H., 2004. Formation and growth rates of ultrafine atmospheric particles: a review of observations. J. Aerosol Sci. 35, 143–176.
Kulmala, M., Kontkanen, J., Junninen, H., Lehtipalo, K., Manninen, H.E., Nieminen, T., Petäjä, T., Sipilä, M., Schobesberger, S., Rantala, P., Franchin, A., Jokinen, T., Järvinen, E., Äijälä, M., Kangasluoma, J., Hakala, J., Aalto, P.P., Paasonen, P., Mikkilä, J., Vanhanen, J., Aalto, J., Hakola, H., Makkonen, U., Ruuskanen, T., Mauldin, R.L., Duplissy, J., Vehkamäki, H., Bäck, J., Kortelainen, A., Riipinen, I., Kurtén, T., Johnston, M.V., Smith, J.N., Ehn, M., Mentel, T.F., Lehtinen, K.E.J., Laaksonen, A., Kerminen, V.-M., Worsnop, D.R., 2013. Direct observations of atmospheric aerosol nucleation. Science 339, 943.
Kürten, A., Jokinen, T., Simon, M., Sipilä, M., Sarnela, N., Junninen, H., Adamov, A., Almeida, J., Amorim, A., Bianchi, F., Breitenlechner, M., Dommen, J., Donahue, N. M., Duplissy, J., Ehrhart, S., Flagan, R.C., Franchin, A., Hakala, J., Hansel, A., Heinritzi, M., Hutterli, M., Kangasluoma, J., Kirkby, J., Laaksonen, A., Lehtipalo, K., Leiminger, M., Makhmutov, V., Mathot, S., Onnela, A., Petäjä, T., Praplan, A.P., Riccobono, F., Rissanen, M.P., Rondo, L., Schobesberger, S., Seinfeld, J.H., Steiner, G., Tomé, A., Tröstl, J., Winkler, P.M., Williamson, C., Wimmer, D., Ye, P., Baltensperger, U., Carslaw, K.S., Kulmala, M., Worsnop, D.R., Curtius, J., 2014. Neutral molecular cluster formation of sulfuric acid–dimethylamine observed in real time under atmospheric conditions. Proc. Natl. Acad. Sci. Unit. States Am. 111, 15019.
Kürten, A., Münch, S., Rondo, L., Bianchi, F., Duplissy, J., Jokinen, T., Junninen, H., Sarnela, N., Schobesberger, S., Simon, M., Sipilä, M., Almeida, J., Amorim, A., Dommen, J., Donahue, N.M., Dunne, E.M., Flagan, R.C., Franchin, A., Kirkby, J., Kupc, A., Makhmutov, V., Petäjä, T., Praplan, A.P., Riccobono, F., Steiner, G., Tomé, A., Tsagkogeorgas, G., Wagner, P.E., Wimmer, D., Baltensperger, U., Kulmala, M., Worsnop, D.R., Curtius, J., 2015. Thermodynamics of the formation of sulfuric acid dimers in the binary (H_2SO_4–H_2O) and ternary (H_2SO_4–H_2O–NH_3) system. Atmos. Chem. Phys. 15, 10701–10721.
Kuwata, K., Akiyama, E., Yamazaki, Y., Yamasaki, H., Kuge, Y., 1983. Trace determination of low molecular weight aliphatic amines in air by gas chromatograph. Anal. Chem. 55, 2199–2201.
Lee, S.-H., Gordon, H., Yu, H., Lehtipalo, K., Haley, R., Li, Y., Zhang, R., 2019. New particle formation in the atmosphere: from molecular clusters to. Glob. Clim. 124, 7098–7146.
Li, J., Feng, Y.-J., Jiang, S., Wang, C.-Y., Han, Y.-J., Xu, C.-X., Wen, H., Huang, T., Liu, Y.-R., Huang, W., 2019. Hydration of acetic acid-dimethylamine complex and its atmospheric implications. Atmos. Environ. 219, 117005.
Licht, W., 1977. In: Friedlander, S.K. (Ed.), Smoke, Dust, and Haze Fundamentals of Aerosal Behavior. John Wiley & Sons, 1977. 317 pages. Price: $16.95. AIChE Journal 23, 773-773.
Liu, Y.-R., Wen, H., Huang, T., Lin, X.-X., Gai, Y.-B., Hu, C.-J., Zhang, W.-J., Huang, W., 2014. Structural exploration of water, nitrate/water, and oxalate/water clusters with Basin-Hopping method using a compressed sampling technique. J. Phys. Chem. A 118, 508–516.
Loukonen, V., Kurtén, T., Ortega, I.K., Vehkamäki, H., Pádua, A.A.H., Sellegri, K., Kulmala, M., 2010. Enhancing effect of dimethylamine in sulfuric acid nucleation in the presence of water – a computational study. Atmos. Chem. Phys. 10, 4961–4974.
Matsumoto, K., Uematsu, M., 2005. Free amino acids in marine aerosols over the western North Pacific Ocean. Atmos. Environ. 39, 2163–2170.
McGrath, M.J., Olenius, T., Ortega, I.K., Loukonen, V., Paasonen, P., Kurtén, T., Kulmala, M., Vehkamäki, H., 2012. Atmospheric Cluster Dynamics Code: a flexible method for solution of the birth-death equations. Atmos. Chem. Phys. 12, 2345–2355.
McGregor, K.G., Anastasio, C., 2001. Chemistry of fog waters in California's Central Valley: 2. Photochemical transformations of amino acids and alkyl amines. Atmos. Environ. 35, 1091–1104.
Meehl, G.A., 1996. Climate change from increased CO2 and direct and indirect effects of sulfate aerosols. Geophys. Res. Lett. 23, 3755–3758.
Merikanto, J., Spracklen, D.V., Mann, G.W., Pickering, S.J., Carslaw, K.S., 2009. Impact of nucleation on global CCN. Atmos. Chem. Phys. 9, 8601–8616.
Milne, P.J., Zika, R.G., 1993. Amino acid nitrogen in atmospheric aerosols: occurrence, sources and photochemical modification. J. Atmos. Chem. 16, 361–398.
Neese, F., 2018. Software update: the ORCA program system, version 4.0. WIREs Comput. Mol. Sci. 8, e1327.
O'Dowd, C.D., Aalto, P., Hämeri, K., Kulmala, M., Hoffmann, T., 2002a. Atmospheric particles from organic vapours. Nature 416, 497–498.
O'Dowd, C.D., Jimenez, J.L., Bahreini, R., Flagan, R.C., Seinfeld, J.H., Hämeri, K., Pirjola, L., Kulmala, M., Jennings, S.G., Hoffmann, T., 2002b. Marine aerosol formation from biogenic iodine emissions. Nature 417, 632–636.
Olenius, T., Kupiainen-Määttä, O., Ortega, I.K., Kurtén, T., 2013. Free energy barrier in the growth of sulfuric acid–ammonia and sulfuric acid–dimethylamine clusters. J. Chem. Phys. 139, 084312.
Ortega, I.K., Kupiainen, O., Kurtén, T., Olenius, T., Wilkman, O., McGrath, M.J., Loukonen, V., Vehkamäki, H., 2011. From quantum chemical formation free energies to evaporation rates, 11, 27327.
Ortega, I.K., Kupiainen, O., Kurtén, T., Olenius, T., Wilkman, O., McGrath, M.J., Loukonen, V., Vehkamäki, H., 2012. From quantum chemical formation free energies to evaporation rates. Atmos. Chem. Phys. 12, 225–235.
Raes, F., Dingenen, R.V., Vignati, E., Wilson, J., Putaud, J.-P., Seinfeld, J.H., Adams, P., 2000. Formation and cycling of aerosols in the global troposphere. Atmos. Environ. 34, 4215–4240.
Ren, L., Bai, H., Yu, X., Wu, F., Yue, S., Ren, H., Li, L., Lai, S., Sun, Y., Wang, Z., Fu, P., 2018. Molecular composition and seasonal variation of amino acids in urban aerosols from Beijing, China. Atmos. Res. 203, 28–35.
Riplinger, C., Neese, F., 2013. An efficient and near linear scaling pair natural orbital based local coupled cluster method. J. Chem. Phys. 138, 034106.
Rosser, F., Forno, E., Kurland, K.S., Han, Y.-Y., Mair, C., Acosta-Pérez, E., Canino, G., Celedón, J.C., 2020. Annual SO2 exposure, asthma, atopy, and lung function in Puerto Rican children. Pediatr. Pulmonol. 55, 330–337.
Satheesh, S.K., Krishna Moorthy, K., 2005. Radiative effects of natural aerosols: a review. Atmos. Environ. 39, 2089–2110.
Saxon, A., Diaz-Sanchez, D., 2005. Air pollution and allergy: you are what you breathe. Nat. Immunol. 6, 223–226.
Sipilä, M., Berndt, T., Petäjä, T., Brus, D., Vanhanen, J., Stratmann, F., Patokoski, J., Mauldin, R.L., Hyvärinen, A.-P., Lihavainen, H., Kulmala, M., 2010. The role of sulfuric acid in atmospheric nucleation. Science 327, 1243.
Smith Jr., W.L., Hansen, C., Bucholtz, A., Anderson, B.E., Beckley, M., Corbett, J.G., Cullather, R.I., Hines, K.M., Hofton, M., Kato, S., Lubin, D., Moore, R.H., Segal Rosenhaimer, M., Redemann, J., Schmidt, S., Scott, R., Song, S., Barrick, J.D., Blair, J.B., Bromwich, D.H., Brooks, C., Chen, G., Cornejo, H., Corr, C.A., Ham, S.-H., Kittelman, A.S., Knappmiller, S., LeBlanc, S., Loeb, N.G., Miller, C., Nguyen, L., Palikonda, R., Rabine, D., Reid, E.A., Richter-Menge, J.A., Pilewskie, P., Shinozuka, Y., Spangenberg, D., Stackhouse, P., Taylor, P., Thornhill, K.L., van Gilst, D., Winstead, E., 2017. Arctic radiation-IceBridge sea and ice experiment: the arctic radiant energy system during the critical seasonal ice transition. Bull. Am. Meteorol. Soc. 98, 1399–1426.
Song, T., Wang, S., Zhang, Y., Song, J., Liu, F., Fu, P., Shiraiwa, M., Xie, Z., Yue, D., Zhong, L., Zheng, J., Lai, S., 2017. Proteins and amino acids in fine particulate matter in rural Guangzhou, Southern China: seasonal cycles, sources, and atmospheric processes. Environ. Sci. Technol. 51, 6773–6781.
Sun, L., Hede, T., Tu, Y., Leck, C., Ågren, H., 2013. Combined effect of Glycine and sea salt on aerosol cloud droplet activation predicted by molecular dynamics simulations. J. Phys. Chem. A 117, 10746–10752.
Tiszenkel, L., Stangl, C., Krasnomowitz, J., Ouyang, Q., Yu, H., Apsokardu, M.J., Johnston, M.V., Lee, S.H., 2019. Temperature effects on sulfuric acid aerosol nucleation and growth: initial results from the TANGENT study. Atmos. Chem. Phys. 19, 8915–8929.
Wales, D.J., Doye, J.P.K., 1997. Global optimization by Basin-Hopping and the lowest energy structures of Lennard-Jones clusters containing up to 110 atoms. J. Phys. Chem. A 101, 5111–5116.
Wedyan, M.A., Preston, M.R., 2008. The coupling of surface seawater organic nitrogen and the marine aerosol as inferred from enantiomer-specific amino acid analysis. Atmos. Environ. 42, 8698–8705.
Wendisch, M., Macke, A., Ehrlich, A., Lüpkes, C., Mech, M., Chechin, D., Dethloff, K., Velasco, C.B., Bozem, H., Brückner, M., Clemen, H.-C., Crewell, S., Donth, T., Dupuy, R., Ebell, K., Egerer, U., Engelmann, R., Engler, C., Eppers, O., Gehrmann, M., Gong, X., Gottschalk, M., Gourbeyre, C., Griesche, H., Hartmann, J., Hartmann, M., Heinold, B., Herber, A., Herrmann, H., Heygster, G., Hoor, P., Jafariserajehlou, S., Jäkel, E., Järvinen, E., Jourdan, O., Kästner, U., Kecorius, S., Knudsen, E.M., Köllner, F., Kretzschmar, J., Lelli, L., Leroy, D., Maturilli, M., Mei, L., Mertes, S., Mioche, G., Neuber, R., Nicolaus, M., Nomokonova, T., Notholt, J., Palm, M., van Pinxteren, M., Quaas, J., Richter, P., Ruiz-Donoso, E., Schäfer, M., Schmieder, K., Schnaiter, M., Schneider, J., Schwarzenböck, A., Seifert, P., Shupe, M. D., Siebert, H., Spreen, G., Stapf, J., Stratmann, F., Vogl, T., Welti, A., Wex, H., Wiedensohler, A., Zanatta, M., Zeppenfeld, S., 2019. The arctic cloud puzzle: using ACLOUD/PASCAL multiplatform observations to unravel the role of clouds and aerosol particles in arctic amplification. Bull. Am. Meteorol. Soc. 100, 841–871.
Wu, Z., Hu, M., Liu, S., Wehner, B., Bauer, S., Ma ßling, A., Wiedensohler, A., Petäjä, T., Dal Maso, M., Kulmala, M., 2007. New Particle Formation in Beijing, China: Statistical Analysis of a 1-year Data Set, vol. 112.
Xie, H.-B., Elm, J., Halonen, R., Myllys, N., Kurtén, T., Kulmala, M., Vehkamäki, H., 2017. Atmospheric fate of monoethanolamine: enhancing new particle formation of sulfuric acid as an important removal process. Environ. Sci. Technol. 51, 8422–8431.
Xu, W., Zhang, R., 2012. Theoretical investigation of interaction of dicarboxylic acids with common aerosol nucleation precursors. J. Phys. Chem. A 116, 4539–4550.
Xu, Y., Wu, D., Xiao, H., Zhou, J., 2019. Dissolved hydrolyzed amino acids in precipitation in suburban Guiyang, southwestern China: seasonal variations and potential atmospheric processes. Atmos. Environ. 211, 247–255.
Xu, C.-X., Jiang, S., Liu, Y.-R., Feng, Y.-J., Wang, Z.-H., Huang, T., Zhao, Y., Li, J., Huang, W., 2020. Formation of atmospheric molecular clusters of methanesulfonic acid–Diethylamine complex and its atmospheric significance. Atmos. Environ. 226, 117404.
Yang, H., Yu, J.Z., Ho, S.S.H., Xu, J., Wu, W.-S., Wan, C.H., Wang, X., Wang, X., Wang, L., 2005. The chemical composition of inorganic and carbonaceous materials in PM2.5 in Nanjing, China. Atmos. Environ. 39, 3735–3749.
Yao, L., Garmash, O., Bianchi, F., Zheng, J., Yan, C., Kontkanen, J., Junninen, H., Mazon, S.B., Ehn, M., Paasonen, P., Sipilä, M., Wang, M., Wang, X., Xiao, S., Chen, H., Lu, Y., Zhang, B., Wang, D., Fu, Q., Geng, F., Li, L., Wang, H., Qiao, L., Yang, X., Chen, J., Kerminen, V.-M., Petäjä, T., Worsnop, D.R., Kulmala, M., Wang, L., 2018. Atmospheric new particle formation from sulfuric acid and amines in a Chinese megacity. Science 361, 278.
Youn, J.S., Crosbie, E., Maudlin, L.C., Wang, Z., Sorooshian, A., 2015. Dimethylamine as a major alkyl amine species in particles and cloud water: observations in semi-arid and coastal regions. Atmos. Environ. 122, 250–258.
Yu, F., Turco, R.P., 2000. Ultrafine aerosol formation via ion-mediated nucleation. Geophys. Res. Lett. 27, 883–886.

Zhang, Q., Anastasio, C., 2003. Free and combined amino compounds in atmospheric fine particles (PM2.5) and fog waters from Northern California. Atmos. Environ. 37, 2247–2258.
Zhang, R., Suh, I., Zhao, J., Zhang, D., Fortner, E.C., Tie, X., Molina, L.T., Molina, M.J., 2004. Atmospheric new particle formation enhanced by organic acids. Science 304, 1487–1490.
Zhang, R., Khalizov, A., Wang, L., Hu, M., Xu, W., 2012. Nucleation and growth of nanoparticles in the atmosphere. Chem. Rev. 112, 1957–2011.
Zhang, R., Li, Y., Zhang, A.L., Wang, Y., Molina, M.J., 2020. Identifying airborne transmission as the dominant route for the spread of COVID-19. Proc. Natl. Acad. Sci. Unit. States Am. 117, 14857.